Review Article

Artifacts and artifact removal in optical coherence tomographic angiography

Tristan T. Hormel[1], David Huang[1], Yali Jia[1,2]

[1]Casey Eye Institute, Oregon Health & Science University, Portland, OR, USA; [2]Department of Biomedical Engineering, Oregon Health & Science University, Portland, OR, USA

Correspondence to: Yali Jia. Casey Eye Institute, Oregon Health & Science University, Portland, OR, USA. Email: jiaya@ohsu.edu.

Abstract: Optical coherence tomographic angiography (OCTA) enables rapid imaging of retinal vasculature in three dimensions. While the technique has provided quantification of healthy vessels as well as pathology in several diseases, it is not unusual for OCTA data to contain artifacts that may influence measurement outcomes or defy image interpretation. In this review, we discuss the sources of several OCTA artifacts—including projection, motion, and signal reduction—as well as strategies for their removal. Artifact compensation can improve the accuracy of OCTA measurements, and the most effective use of the technology will incorporate hardware and software that can perform such correction.

Keywords: Optical coherence tomographic angiography (OCTA); imaging artifacts; artifact correction

Submitted Jun 04, 2020. Accepted for publication Jul 29, 2020.
doi: 10.21037/qims-20-730
View this article at: http://dx.doi.org/10.21037/qims-20-730

Introduction

Optical coherence tomographic angiography (OCTA) (1-3) provides high-resolution, depth-resolved, non-invasive visualization of vasculature. The technique leverages the fluctuation in signal between consecutive OCT cross-sectional scans caused by flowing blood as an inherent contrast in order to detect vessels down to the capillary scale. While the technique has been applied to image skin (1,4,5), mouse brains (6,7), and developing zebrafish embryos (8), it has so far been most widely used in ophthalmic imaging and eye research (9-11), where it has provided insight into the vascular morphology of healthy eyes (12) and eyes afflicted by vision-threatening diseases such as age-related macular degeneration (AMD) (13-20), diabetic retinopathy (DR) (21-24), glaucoma (25-28), and others (29-34). In this context, researchers have found that image-based measurements commonly made on OCTA, such as vessel density and avascular area, can distinguish between healthy and pathological eyes (22,31,35-37) and sometimes with better accuracy than alternative imaging modalities (38).

While these advantages have led to its rapid adoption as a research tool and in the clinic, as an emerging technology OCTA still suffers some limitations. For example, OCTA fields of view are typically much smaller than those in other angiographic techniques, such as fluorescein angiography (FA) or indocyanine green angiography (ICGA), employed in ophthalmology. This drawback means that pathology that manifests in the peripheral retina may not always be revealed by OCTA. However, the most prominent limitations in OCTA are imaging artifacts. While some artifacts are innocuous or easily detectable, others can be severe while still remaining subtle. Measurement accuracy on OCTA data can be reduced by artifacts, and in the worst cases they can even suggest misleading conclusions. Currently artifacts are common, with one study reporting their presence in 97% of OCTA images (39). It is essential, then, that anyone working with OCTA data understand their effects.

In this review, we will examine the source of OCTA artifacts, including projection, bulk motion, and signal reduction. In order to illuminate the origin of these artifacts we will first discuss signal generation in OCTA.

Flow signal and confounding factors

Flow signal in OCTA is derived from motion contrast between consecutive OCT B-scans. The OCT signal itself is acquired through coherence gating, where interference with a reference arm amplifies the signal from the sample arm in order to resolve the depth at which the signal originates. Contemporary OCT systems replace the original time-domain processing, which required the physical scanning of a reference mirror, with Fourier-domain processing. For illumination from a light source with Gaussian power spectral density, this signal within a line scan at a depth z can be succinctly written (40)

$$\mathfrak{F}^{-1}\{I(k)\}(z) = A(z)\exp\left[-i\Phi(z)\right] \quad [1]$$

where $\mathfrak{F}^{-1}\{I(k)\}(z)$ denotes the inverse Fourier transform of the detected signal in k-space at depth z, and $A(z)$ and $\Phi(z)$ denote the amplitude and phase of the signal, respectively. As indicated by Eq. [1], motion contrast can manifest in both the phase and amplitude of the complex OCT signal. Consequently, OCTA can be generated by examining motion contrast in the phase, amplitude, or complex signal (41). It is often claimed that phase contrast measurements are more sensitive to slow flow (41,42); however, phase signals need be stabilized or compensated by correcting the bulk motion-generated phase shift before computing OCTA signals. Thus, phase, or complex-signal-based OCTA algorithms are highly dependent on an appropriate phase compensation step (43). Despite these differences, they are largely immaterial in the context of retinal imaging, where flow in capillaries is detectable using either amplitude or phase. Both amplitude and complex-signal-based OCTA approaches can detect very slow flow (including Brownian motion), such as the *in vitro* intralipid flow when syringe pumps stop (44,45) or the *in vivo* flow in intraretina cystic spaces (46,47). Most commercial instruments (Optovue, Topcon, and Heidelberg) are amplitude-based, while Zeiss uses complex-signal processing.

In addition to the specifics of the signal being processed to construct OCTA data, the mathematics used to quantify signal variation can also influence the presence of image artifacts. Common approaches include difference, variance, and (de)correlation. To gain an intuition for how the choice of motion contrast metric influences OCTA image generation, we can consider two prominent OCTA construction techniques. In optical microangiography (OMAG) (1), the flow signal is calculated from the complex signal as

$$I_{\mathrm{OMAG}}(x,z) = \left[I_{n+1}(x,z) - I_n(x,z)\right]_{\mathrm{ABS}} \quad [2]$$

where I_n is value of the nth cross-sectional scan at location (x,z), and $[\xi]_{\mathrm{ABS}}$ indicates magnitude of ξ. In contrast, split-spectrum amplitude decorrelation angiography (SSADA) (2) uses decorrelation instead of difference:

$$D(x,z) = 1 - \frac{1}{N-1}\frac{1}{M}\sum_{n=1}^{N-1}\sum_{m=1}^{M}\frac{A_{m,n}(x,z)A_{m,n+1}(x,z)}{\frac{1}{2}A_{m,n}(x,z)^2 + \frac{1}{2}A_{m,n+1}(x,z)^2} \quad [3]$$

where A_n represents the amplitude of the nth cross-sectional scan at (x,z). SSADA also employs the split-spectrum approach wherein the OCT spectrum is calculated across M sub-bands; the decorrelation in each sub-band is averaged to form the final decorrelation value, thereby increasing the signal-to-noise ratio. It is easily seen that D does not scale with the magnitude of A: if $A_{m,n}$ (x,z) and $A_{m,n+1}$ (x,z) differ by 20%, doubling the value of both will not change the value of D (x,z). On the other hand, if I_n (x,z) and I_{n+1} (x,z) also differ by 20%, doubling both their values will preserve a 20% ratio, but the value of I_{OMAG} (x,z) will have doubled. This example elucidates the point that in difference (and variance) methods the flow signal is more strongly coupled to the magnitude of the OCT signal than in decorrelation-based methods. This makes correlation/decorrelation approaches less likely to misdetect flow in hyperreflective material. Alternatively, since noise is maximally decorrelated, low signal regions in which noise predominates register a large decorrelation value. For this reason, correlation-based approaches introduce amplitude or phase cutoffs that prevent flow detection in hyporeflective regions. This re-introduces a reflectance magnitude dependence into these approaches.

Projection artifacts

Independent of the specifics of processing, by virtue of being generated from OCT data all OCTA flow signal acquires depth resolution through coherence gating. This idea can be written explicitly into Eq. [1] as

$$\mathfrak{F}^{-1}\{I(k)\}(z) = 2r_R I_0 \sum_{n=1}^{N} r_S(\ell_n)\gamma\left[2z-\ell_n\right]e^{-ik_0(2z-\ell_n)} \quad [4]$$

where r_R and r_S represent the reflectance of the reference and sample, respectively, I_0 is the intensity of the

illuminating beam, $\exp\left[-ik_0\left(2z-\ell_n\right)\right]$ represents the phase, and $\gamma\left[2z-\ell_n\right]$ is the temporal autocorrelation accounting for coherence gating for a scattering event with path length ℓ (41). The summation over n accounts for the fact that the OCT signal is in general composed of N scattering events. The principle that enables depth resolution in OCT is that at any location the majority of these detected photons will be the result of backscattering from single scattering events, in which case the path length ℓ_n is can be written $\ell_n = 2z_n$, with the criterion for detection due to coherence gating that $z_n \approx z$. However, multiple scattering events can also contribute to the summation in Eq. [4] provided the total path length still sums to $\ell_n \approx 2z_n$. Our experience with structural OCT informs us that the largest contribution to I is indeed from single backscattering events. In the context of OCTA specifically, it is worth noting that simulations indicate that red blood cells forward scatter light with relatively high probability (48,49). Such forward scattered photons can be subsequently backscattered. Forward scattering from moving red blood cells varies temporally, just as backscattering does. When photons forward-scattered by a red blood cells are subsequently back-scattered by deeper tissue they will contribute to flow signal detectable by OCTA.

The result of such multiple scattering events are projection artifacts. Arguably the most pernicious source of confusion in OCTA interpretation and analysis, they have the unfortunate capacity to mimic the appearance of real vasculature (*Figure 1*). Because they are largely the result of forward scattering, projection artifacts replicate the signal from superficial vasculature in deeper tissue. They are typically most prevalent near strongly back scattering tissue (such as the retinal pigment epithelium), since such material will reflect more of the forward-scattered photons that produce the artifacts. When this spurious signal appears in deeper vascular regions, for example when signal from the superficial vascular complex (SVC) is projected into the deep capillary plexus (DCP), it can reduce the accuracy of important OCTA measurements in such regions. Vessel density measurements from deeper plexuses made without projection artifact removal, as for instance in refs. (31,50-53), are not simply measurements from the plexus they were performed on, but some weighted amalgam of that plexus and more superficial vessels. Vessel density is not alone in this concern; any measurements extracted from vasculature in deeper layers will likewise conflate features from superficial plexuses and complexes. Other metrics, such as non-perfusion area, are disturbed even more by projection artifacts since artifactual flow signal can introduce signal into regions that are flow-free. These projection artifacts prevent us from detecting actual non-perfusion areas associated with diabetic retinopathy or retinal degeneration. Similarly, projection artifacts are especially problematic for detection and quantification of choroidal neovascularization (CNV) (*Figure 2*). As CNV erupts into the normally avascular outer retina, it could be detected by noticing flow in that region; however, projection artifacts can complicate this observation by introducing signal that must be separated from true flow in order to correctly ascertain the presence of CNV. Since the appearance of CNV is a major indicator in treatment of age-related macular degeneration (AMD) (13,54), accurate quantification of this development is extremely important from a clinical perspective; but at the same time, projection artifacts are often severe in the outer retina due to large amount of back scattered signal from the retinal pigment epithelium.

In addition to replicating superficial vascular features in deeper anatomic slabs, projection artifacts also produce "tails" on vessels in cross-sectional images (*Figure 1*). These tails can make determination of the depth of the CNV lesion problematic, and therefore infringe on our ability to determine CNV type. The artifactual tails also interfere substantially with visualization of retinal angiomatous proliferation, since they can mask real vessels connecting retinal and choroidal circulation as well as produce spurious signal that looks like such vessels (55).

One simple means of removing projection artifacts is slab subtraction (3,20,56). In this approach, the signal in superficial plexuses or complexes is subtracted, possibly after weighting, from angiograms in deeper tissue. This operation has the advantage of unambiguously removing projection artifacts, but also has several drawbacks. For one, real flow signal that happens to coincide with the projection artifact signal will also be removed. This means that slab subtraction cannot rescue measurements of vessel density in the DCP, since slab-subtracted angiograms would lead to underestimates in the same way un-modified angiograms with projection artifacts present would lead to over-estimates. Other OCTA metrics are similarly affected by this approach, with vessel connectivity in particular suffering. For this reason, slab subtraction is best applied for measurements performed in avascular regions. But even in such regions other measurements we might be interested in, for example CNV morphology, will be disrupted. An additional limitation is that slab subtraction

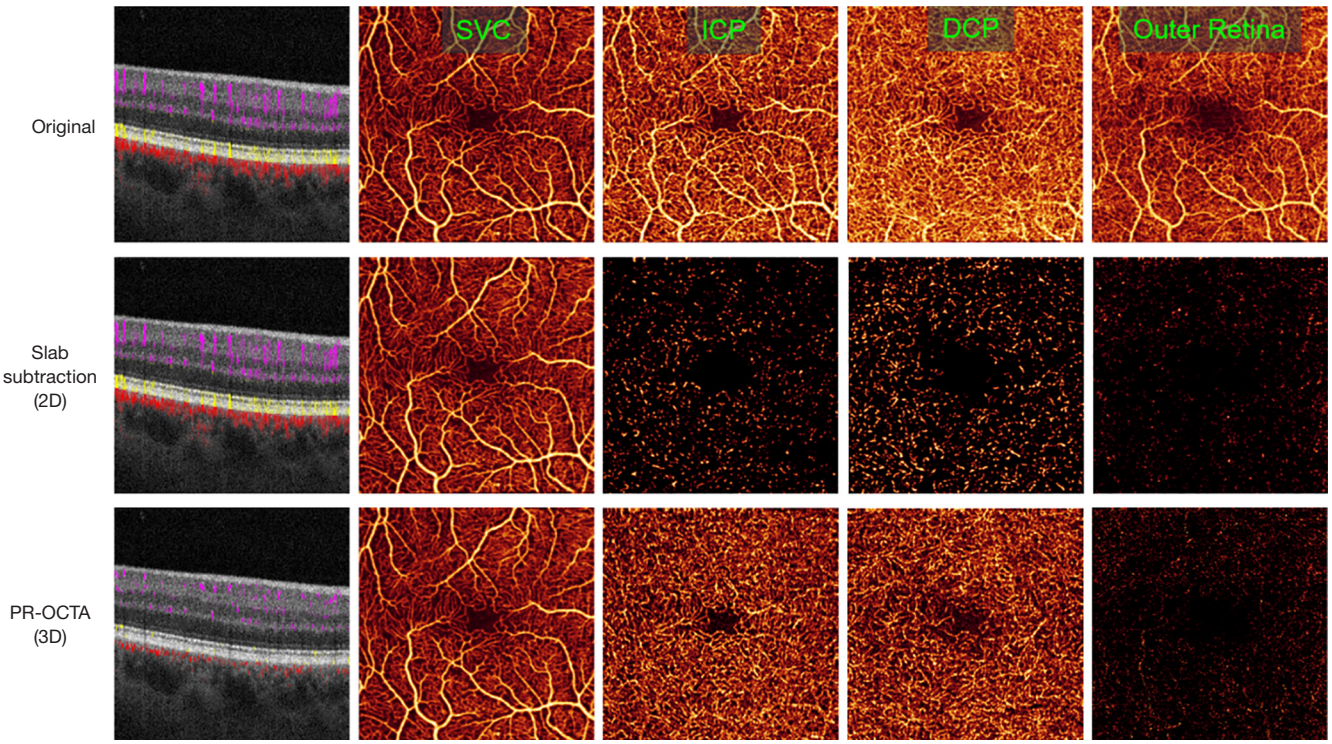

Figure 1 Comparison of retinal optical coherence tomographic angiography (OCTA) (3×3 mm^2) from a healthy volunteer showing an uncorrected scan (row 1), shadow artifact removal from slab subtraction (row 2), and with projection resolution (PR-OCTA; row 3). Shown are merged structural and OCTA cross-sectional images (column 1) and en face OCTAs for the superficial vascular complex (SVC; column 2), intermediate capillary plexus (ICP; column 3), deep capillary plexus (DCP; column 4), and outer retina (column 5). The projection artifacts are especially prominent in the outer retina, which is avascular in healthy individuals (column 4, top row); the same flow pattern is also clearly visible in the ICP slab (column 2 top row). Projection artifacts also cause vessels in cross-section to appear as vertical strips (top left) rather than as the anatomically accurate dots as imaged by PR-OCTA. As can be seen from the cross-sectional image, while slab subtraction does remove projection artifacts from the en face images, it is not a three-dimensional technique, and so vessel tails are not removed. Slab subtraction also disrupts vessel continuity, as can be seen in the slab-subtracted ICP and DCP images. In the cross-sectional images, flow signal is colored coded according to location in the inner retina (violet), outer retina (yellow), and choroid (red). Slab definitions are SVC: from the nerve fiber layer to 67% of the way through the ganglion cell layer and inner plexiform layer; ICP: from the bottom of the SVC to midway through the inner nuclear layer; DCP: from the bottom of the ICP through the outer plexiform layer; outer retina: from the bottom of the outer plexiform layer to Bruch's membrane. Collectively the SVC, ICP, and DCP form the inner retina.

operates exclusively on *en face* images. It cannot be used to remove the tails that projection artifacts introduce to vessels in cross-section. Finally, slab subtraction also requires accurate slab segmentation (from which to determine what signal should be removed from deeper layers). Correct slab segmentation is often difficult without intelligent algorithms, such as in (57,58), especially when eyes are affected by pathology—i.e., precisely when we typically employ OCTA in the first place. When slabs aren't properly segmented, slab subtracted angiograms may incorporate flow signal removal that doesn't even correspond to features from superficial layers.

A better approach for removing projection artifacts is projection-resolved OCTA (PR-OCTA) (59,60) (*Figure 1*). PR-OCTA algorithms are based on the observation that reflectance-normalized signal in projection artifacts is smaller than that of true *in situ* flow in overlying voxels in the same axial line. Specifically, the structural OCT signal is used to weigh the flow signal in OCTA volume, and the algorithm keeps the flow values at the successively higher peaks (*in situ* flow) along each A-line and suppress the rest to background level. Since this

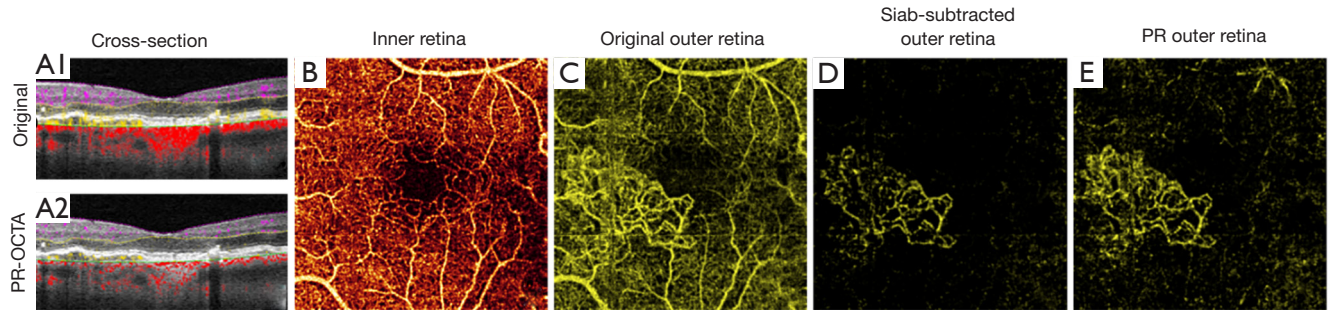

Figure 2 Choroidal neovascularization as imaged by different methods for projection artifact removal. Cross-sections show flow signal (violet: inner retinal; yellow: outer retinal; red: choroidal flow) overlaid on structural optical coherence tomographic (OCT). (A1) original optical coherence tomographic angiography (OCTA) and (A2) projection-resolved OCTA (PR-OCTA). Artifactual tails that cause vessels to appear as vertical lines, rather than dots in cross-section, are clearly visible in the uncorrected image. (B) The superficial vascular complex slab. (C) Original OCTA angiogram of the outer retina. In a healthy eye, this slab is avascular, but choroidal neovascularization (CNV) is visible here, though heavily obscured by projection artifacts. The projection artifacts mimic the appearance of the superficial vasculature. (D) The same slab, after slab subtraction projection artifact removal. While the projection artifacts are removed, the vessels within the CNV lesion are disrupted, which may hinder some quantification. (E) The same slab viewed with PR-OCTA. While some residual projection artifacts are visible, the vessels in the CNV lesion remain continuous. Slab definitions are SVC: from the nerve fiber layer to 67% of the way through the ganglion cell layer and inner plexiform layer; ICP: from the bottom of the SVC to midway through the inner nuclear layer; DCP: from the bottom of the ICP through the outer plexiform layer; outer retina: from the bottom of the outer plexiform layer to Bruch's membrane. Collectively the SVC, ICP, and DCP form the inner retina.

operation can be performed volumetrically, PR-OCTA has the additional capability of removing projection artifact tails from cross-sectional images. While PR-OCTA generally yields cleaner volumes that slab subtraction, it does still have some limitations. In low quality scans PR-OCTA can retain more residual artifacts than slab subtraction in the outer retina- however, PR-OCTA will not, like slab subtraction, disrupt the morphology of pathological vessels that may be present there. For this reason, it can be useful to rely on a suite of *en face* images including both PR-OCTA and slab subtraction to help more fully characterize projection artifacts, as in for example a recent automated choroidal neovascularization detection algorithm (17). PR-OCTA has also only been tested in an ophthalmological context. While the principles on which it relies should enable the technique to work in other tissues, this remains unverified.

Beyond these published approaches, commercial instruments now also include projection artifact removal algorithms. As these methods are proprietary, their specifics are not covered in this review. However, given that any OCTA image may contain residual artifacts, it is still important to inspect them.

The removal of projection artifacts allows retinal plexuses and complexes to be individually visualized (12). This capability enables more refined observation of pathological developments, and from PR-OCTA we now know that several diseases manifest differently in different plexuses (61). For instance, in glaucoma capillary loss primarily affects the superficial vascular complex, with relative sparing of deeper plexuses (26,62). The opposite is true in retinitis pigmentosa, where the deep capillary plexus is most severely affected (32,35,63,64). Even in diabetic retinopathy or vessel occlusions, in which all retinal plexuses suffer capillary drop out, the patterns of loss vary by plexus (37,65-67). PR-OCTA specifically is also particularly useful for imaging CNV, as it allows precise determination of lesion depth and can therefore distinguish CNV type (18,68,69); this is more difficult to achieve with projection removal techniques that do not operate volumetrically. Additionally, PR-OCTA can detect vascular connections between the choroidal and retinal circulations, and so is also advantageous for staging macular telangiectasia and retinal angiomatous proliferation (55,61,70).

Eye motion

Blood flow is not the only source of motion in the eye, and any motion contrast can produce OCTA signal. Such motion has several origins that can manifest differently.

Microsaccades occur every few seconds, which is the

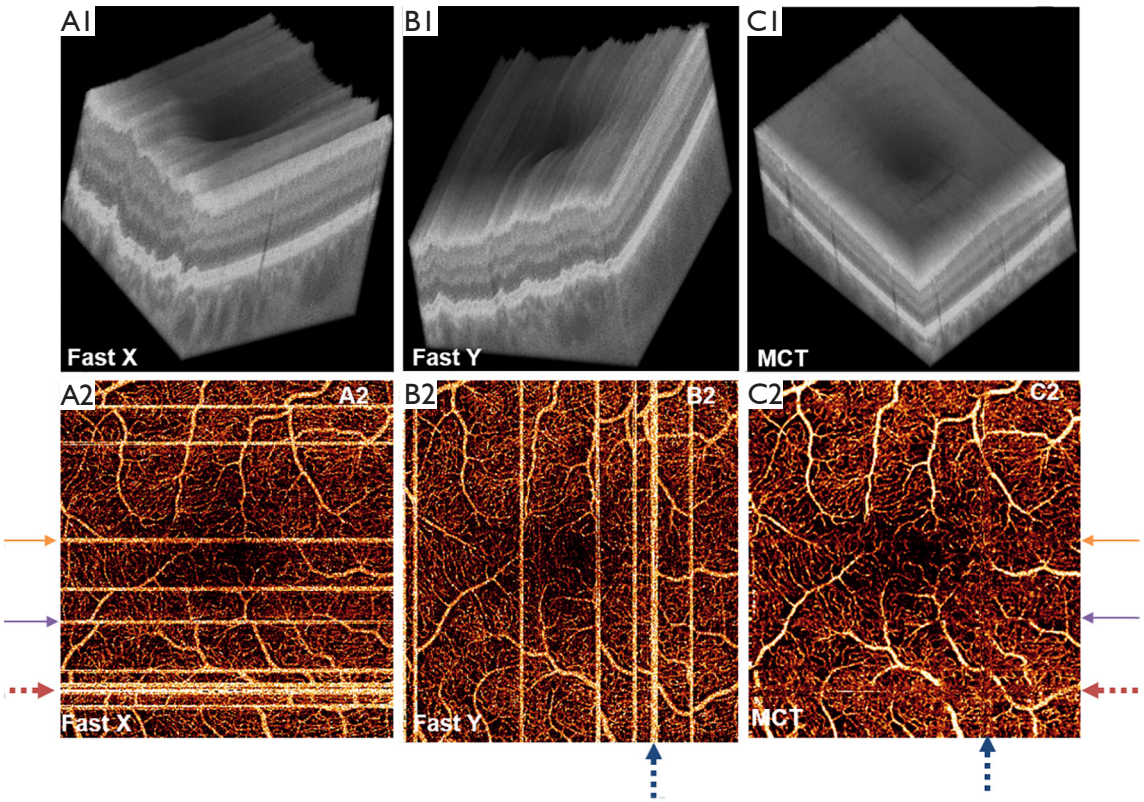

Figure 3 x-fast and y-fast optical coherence tomographic angiography (OCTA) registration. Top row: OCT reflectance volumes completed in an (A) x-fast and (B) y-fast direction, and (C) the volume obtained by registering and merging these volumes (labeled MCT, for motion corrected technology). Bottom row: en *face* OCTA images corresponding to these volumes. In (D) and (E), the bright stripes are due to microsaccades; these artifacts are removed by the registration technique. Reprinted with permission from (71).

same time scale as a complete OCTA data acquisition. For this reason, they are often present in OCTA B-frames. They manifest as bright stripes in *en face* OCTA (*Figure 3*). Both hardware and software solutions can remove these stripes. Real-time tracking allows detection of microsaccades during OCTA acquisition; when microsaccades are detected instruments can rescan the affected location (72-76). Microsaccadic signal can be removed in software by omitting the affected scans (71,77). Instead, if multiple volumes are available, they can be registered and merged to recover the lost B-frames (77,78-81). This solution obviates the need for rescanning, and is often performed by scanning separately along each lateral scanning axis in the fast direction (i.e., x-fast and y-fast scanning schemes; *Figure 3*). Finally, real-time tracking of eye movement can be used to track and rescan areas affected by microsaccades when necessary (72-74). While this approach may increase the duration of imaging sessions some, it can be used to completely remove microsaccadic artifacts. Most tracking software relies on auxiliary technology (for instance, scanning laser ophthalmoscope), although a recent study has demonstrated real time tracking that relies solely on OCTA data (82).

Ocular pulsation or drift are also sources of bulk motion. Like microsaccades, these are common disruptions in OCTA imaging, so they are a common issue in OCTA. The velocity due to this variety of bulk motion can be slow enough that it does not seriously jeopardize OCTA vessel contrast, but this is not always the case. Bulk motion of this variety produces phase noise, and so it is in particular a concern for complex- and phase-based OCTA processing. It is essential for these approaches that the phase noise due to bulk motion be removed before OCTA computation.

These approaches to compensating for bulk motion relied on the observation that in any given OCTA volume, most voxels will be avascular. The bulk motion contribution can then be reasonably estimated by considering statistics of the measured flow signal across all voxels. Several different

approaches are possible based off of this observation; one of the earliest, due to Makita *et al.* with a phase-based OCTA method (83), constructed histograms of the phase-shift value between adjacent line-scans. They used the mode of this distribution as an estimate of the bulk motion contribution. An and Wang, in a complex-signal-based approach, instead used average phase change along a line-scan as the bulk motion contribution method (84). A subtlety for this approach is that a suitable threshold must be applied to remove phase noise, which averages to zero. Inclusion of phase noise in the bulk motion estimate, then, would tend to lead to underestimates. A similar problem occurs with phase wrapping. As OCTA transitioned from measuring motion contrast between subsequent line scans to motion contrast between subsequent cross-sectional scans, the time between scans increased, which had the incidental consequence of introducing a phase ambiguity into phase contrast measurements. This again leads to an underestimate since we can only measure phase within $[-\pi, \pi]$. A standard-deviation-based approach (43) or iterated averaging (85) can resolve this ambiguity and remove this contribution to bulk motion noise.

What all of these approaches have in common is that they appeal to a single test statistic (whether mean, mode, or standard deviation) in order to estimate the bulk motion contribution to the motion contrast signal. A more thorough approach at the post-processing level (after OCTA computation) can improve on these results by sampling more of the bulk motion statistics. One such approach is a regression-based approach that removes bulk motion-associated background by fitting flow signal statistics to an estimate of bulk motion signal strength derived from flow phantom experiments (*Figure 4*) (87). This approach achieves a better signal-to-noise ratio contrast than median subtraction approaches, and has shown utility in multiple instruments.

Signal attenuation

Signal strength in OCTA is tied to reflectance magnitude, whether directly (as in Eq. [2] or other reflectance/complex amplitude-based approaches) or indirectly (as in Eq. [3] or other correlation or ratio-based approaches).

Overall signal intensity in images is quantified on many commercial instruments (for instance signal strength index, SSI, from OptoVue). The signal intensity can influence OCTA metrics, and should be compensated for in order to prevent biased measurements (88). Loss of signal across an entire image is often caused by defocus, and is especially detrimental to OCTA measurements that rely on quantifying flow signal intensity (rather than vessel shape, for instance) (89). Vessel density, for example, can exhibit 10% variation within clinically acceptable scans when measurements are made on the same eye under different signal strength conditions (89). In addition to reducing contrast between vessels and background, defocus also broadens vessel width—another source of artificial variation in vessel density. While traditional, filter-based image processing techniques are sensitive to this variation, modern machine-learning-based quantification can avoid mismeasurement due to defocus (17,22). This is important since OCTA data sets often include defocused scans, but the degree of defocus may not always be evident. Beyond defocus, other common sources of global signal attenuation are cataracts and tear film break up. Since the tear film is responsible for some of the focusing power of the eye, its loss during imaging can lead to dimmer images.

In addition to global signal loss, local signal loss also occurs in OCTA imaging. This is often caused by severe signal attenuation beneath hyperreflective material along the beam path. Hyperreflective material may be found in the retina, for instance the hyperreflective foci sometimes observed in diabetic retinopathy (90,91). But shadowing can also be caused by material outside of the retina—for example, vitreous floaters. Vignetting (*Figure 5*) is also another common source of signal dropout. Depending on the degree of signal loss, it may be impossible to recover information like vessel density in a particular region of the OCTA image. When vessel density is calculated for an entire image, local signal loss will of course suppress the global value. However, local signal loss can appear similar to real capillary dropout while still reducing vessel density. This is a challenging issue for traditional hand-crafted image processing algorithms. Fortunately, modern deep-learning-based algorithms have demonstrated a capability to distinguish shadowing artifacts from real pathology (22) (*Figure 5*).

Discussion and future directions

OCTA technology is still in its infancy, and for this reason it is unsurprising that images often exhibit artifacts. As the previous sections indicate, since its introduction we have collectively and iteratively developed better solutions for removing some of the most prominent artifacts. At the same time, these artifacts still exist and can affect OCTA data,

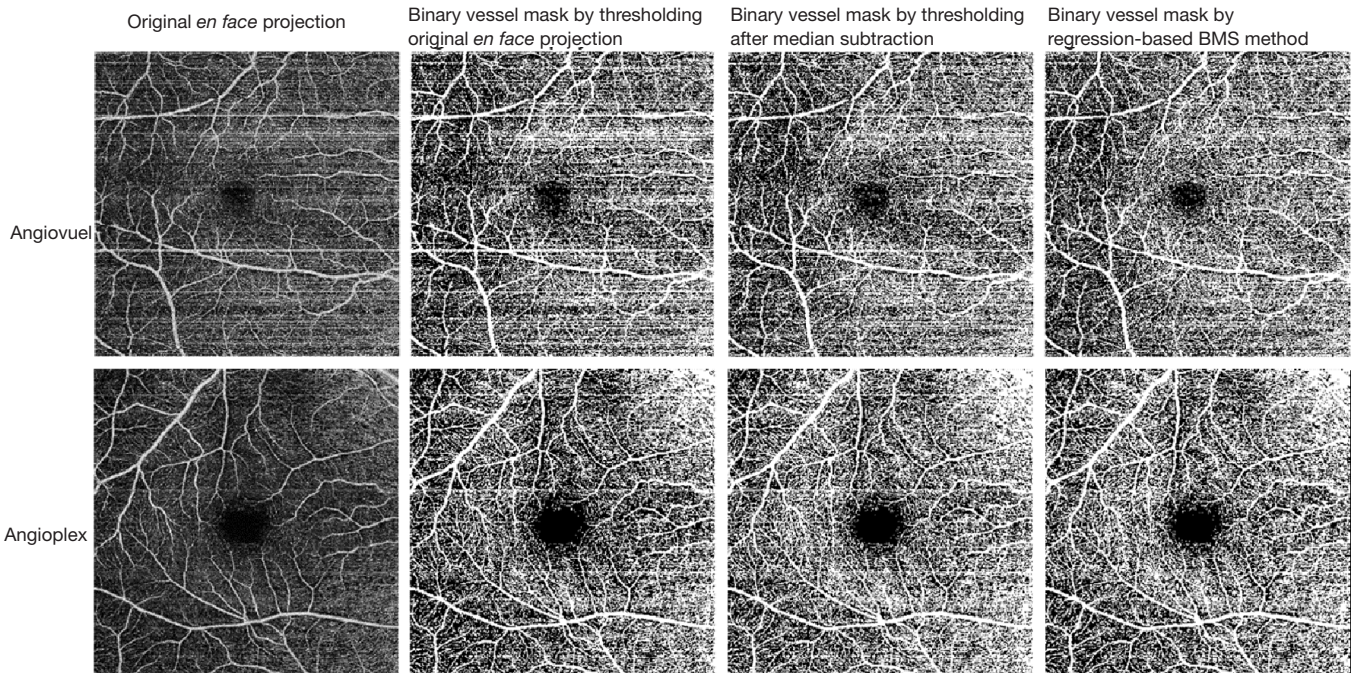

Figure 4 Bulk motion artifact removal on two different optical coherence tomographic (OCT) devices. Top row: AngioVue (OptoVue, USA). Bottom row: AngioPlex (Zeiss, Germany). The first column on the left shows the original *en face* projection of the superficial vascular complex (SVC). The remaining columns show binarization of the raw data (second column), binarization after median subtraction (third column), and after regression-based bulk motion subtraction (last column). Note the prominent horizontal motion artifacts incorporated into the vessel masks created from the original and median-subtracted images (columns 2 and 3) that are removed by the regression-based method (column 4). For slab definitions see the caption to *Figure 1*. Reprinted with permission from (86).

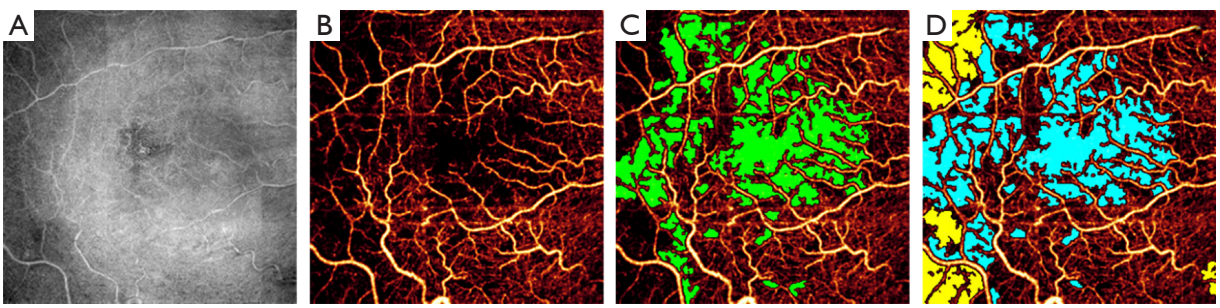

Figure 5 Automated avascular area detection. (A) Reflectance optical coherence tomographic (OCT) image, with shadow artifacts visible to the left. (B) Optical coherence tomographic angiography (OCTA) image of the superficial vascular complex (SVC), with some apparently avascular area actually caused by shadow artifacts. (C) Manually graded ground avascular area (green) overlaid on the angiogram. (D) Artificial intelligence produced avascular area (blue) and area identified as shadow artifact (yellow) by the algorithm. For slab definitions see the caption to *Figure 1*. Reprinted from Guo *et al.* (22).

even with state of the art removal techniques. Can we do better?

Even without significant investment in new technology we are likely to see reduction in some artifacts as OCTA components improve. Faster lasers, such as swept source, vertical-cavity surface-emitting laser that could be incorporated into new instruments are arriving without any effort on the part of the OCTA community. Increased

scanning speeds will reduce bulk motion artifacts of their own accord, and also reduce the number of microsaccade line artifacts present in images by reducing the overall procedure time. However, acquisition speed ultimately competes with flow detection, since the dynamic range in OCTA systems is set in part by the time between B-scans, with shorter inter-frame times becoming decreasingly sensitive to slow flow (92). Instead, real-time tracking could be improved to remove bulk motion artifacts. Here the limiting step is GPU processing or data transfer speeds. Current state-of-the-art research systems can process OCTA in real time at megahertz scan rates (93-95). With better GPUs, swifter tracking will be able to suppress more bulk motion artifacts.

Incorporating these better components into a new generation of OCTA devices can help reduce motion artifacts. By augmenting OCTA instruments with adaptive optics (96) projection artifacts can also be suppressed. Adaptive optics systems can be used to compensate for aberrations in the eye, increasing system optical resolution and enabling visualization of capillaries at anatomic caliber (rather than the expanded caliber seen in current OCTA systems) (97,98). This has the added benefit of removing projection artifacts, since axial resolution can also be improved with this approach. However, state-of-the-art research instruments that incorporate this technology currently employ reduced fields-of-view in order to keep total imaging times feasible—a limitation that will need to be overcome before they become widely applicable.

Both adaptive optics and improved OCTA acquisition and tracking are means to reduce the number of artifacts in images through hardware. Improvements in software also have the potential to clean artifacts better. Modern deep-learning-based image reconstruction has demonstrated the capability to improve signal-to-noise ratios when generating OCTA data from the measured complex signal (99). In Liu *et al.*, this was achieved by training a network on OCTA generated from 48 consecutive B-frames, and requires 4 input B-frames to perform the reconstruction (100). Lee *et al.* instead reconstruct OCTA from single B-frames, which has the innate advantage of suppressing motion artifacts due to the abbreviated times required to acquire one (rather the usual two) data volume (101). In principle, both of these networks could have been trained on OCTA images in which artifacts were already suppressed, so that artifact suppression could be learned simultaneously. However, deep learning techniques such as these could introduce new artifacts of their own—Lee *et al.* noted that some capillaries were not correctly displayed by their network, while Liu *et al.* noted that some vessels gained an artifactual "wave" pattern. It is possible that other, more subtle artifacts that go unnoticed by researchers may also be introduced by these approaches.

Deep-learning based image reconstruction is a means by which artifacts in images can be removed; an alternative is to attempt to accurately quantify OCTA data in which artifacts are present (22). Again, deep-learning methods have shown success in this respect—as noted above, networks can learn features that allow them to identify shadow artifacts.

None of the approaches discussed here can alleviate the detrimental effect of artifacts in OCTA on their own, but neither are any mutually exclusive. Future devices incorporating all or some of these advantages will likely be marred by substantially fewer artifacts that current images.

Conclusions

Even if artifacts do still exist in the current state-of-the-art in OCTA, we have made large strides in cleaning them from images and extracting more accurate measurements from images in which they exist. Clinicians and researchers that are aware of how artifacts affect OCTA will best be able to take advantage of this powerful technology.

Acknowledgments

Funding: This work was supported by grants R01EY027833, R01 EY024544, R01 EY023285, R01 EY031394, P30 EY010572 from the National Institutes of Health (Bethesda, MD) and an unrestricted departmental funding grant and William & Mary Greve Special Scholar Award from Research to Prevent Blindness (New York, NY).

Footnote

Provenance and Peer Review: With the arrangement by the Guest Editors and the editorial office, this article has been reviewed by external peers.

Conflicts of Interest: All authors have completed the ICMJE uniform disclosure form (available at http://dx.doi.org/10.21037/qims-20-730). The special issue "Advanced Optical Imaging in Biomedicine" was commissioned by the editorial office without any funding or sponsorship. DH reports grants from NIH, grants, stock ownership, and personal fees from Optovue, Inc., outside the submitted

work. YJ reports grants from NIH, grants and personal fees from Optovue, Inc., grants from RPB foundation, outside the submitted work. These potential conflicts of interest have been reviewed and managed by OHSU. The authors have no other conflicts of interest to declare.

References

1. An L, Qin J, Wang RK. Ultrahigh sensitive optical microangiography for in vivo imaging of microcirculations within human skin tissue beds. Opt Express 2010;18:8220-8.
2. Jia Y, Tan O, Tokayer J, Potsaid B, Wang Y, Liu JJ, Kraus MF, Subhash H, Fujimoto JG, Hornegger J, Huang D. Split-spectrum amplitude-decorrelation angiography with optical coherence tomography. Opt Express 2012;20:4710-25.
3. Jia Y, Bailey ST, Hwang TS, McClintic SM, Gao SS, Pennesi ME, Flaxel CJ, Lauer AK, Wilson DJ, Hornegger J, Fujimoto JG, Huang D. Quantitative optical coherence tomography angiography of vascular abnormalities in the living human eye. Proc Natl Acad Sci U S A 2015;112:E2395-402.
4. Xu J, Wei W, Song S, Qi X, Wang RK. Scalable wide-field optical coherence tomography-based angiography for in vivo imaging applications. Biomed Opt Express 2016;7:1905.
5. Nam AS, Chico-Calero I, Vakoc BJ. Complex differential variance algorithm for optical coherence tomography angiography. Biomed Opt Express 2014;5:3822.
6. Jonathan E, Enfield J, Leahy MJ. Correlation mapping method for generating microcirculation morphology from optical coherence tomography (OCT) intensity images. J Biophotonics 2011;4:583-7.
7. Wang RK, An L. Doppler optical micro-angiography for volumetric imaging of vascular perfusion in vivo. Opt Express 2009;17:8926.
8. Chen Y, Trinh LA, Fingler J, Fraser SE. Phase variance optical coherence microscopy for label-free imaging of the developing vasculature in zebrafish embryos. J Biomed Opt 2016;21:126022.
9. Kashani AH, Chen CL, Gahm JK, Zheng F, Richter GM, Rosenfeld PJ, Shi Y, Wang RK. Optical coherence tomography angiography: A comprehensive review of current methods and clinical applications. Prog Retin Eye Res 2017;60:66-100.
10. Spaide RF, Fujimoto JG, Waheed NK, Sadda SR, Staurenghi G. Optical coherence tomography angiography. Prog Retin Eye Res 2018;64:1-55.
11. Gao SS, Jia Y, Zhang M, Su JP, Liu G, Hwang TS, Bailey ST, Huang D. Optical Coherence Tomography Angiography. Invest Ophthalmol Vis Sci 2016;57:OCT27-36.
12. Campbell JP, Zhang M, Hwang TS, Bailey ST, Wilson DJ, Jia Y, Huang D. Detailed Vascular Anatomy of the Human Retina by Projection-Resolved Optical Coherence Tomography Angiography. Sci Rep 2017;7:42201.
13. Schmidt-Erfurth U, Klimscha S, Waldstein SM, Bogunovi H. A view of the current and future role of optical coherence tomography in the management of age-related macular degeneration. Eye 2017;31:26-44.
14. Schneider EW, Fowler SC. Optical coherence tomography angiography in the management of age-related macular degeneration. Curr Opin Ophthalmol 2018;29:217-25.
15. Ma J, Desai R, Nesper P, Gill MM, Fawzi A, Skondra D. Optical Coherence Tomographic Angiography Imaging in Age-Related Macular Degeneration. Ophthalmol Eye Dis 2017;9:1179172116686075.
16. Camino A, Guo Y, You Q, Wang J, Huang D, Bailey ST, Jia Y. Detecting and measuring areas of choriocapillaris low perfusion in intermediate, non-neovascular age-related macular degeneration. Neurophotonics 2019;6:041108.
17. Wang J, Hormel TT, Gao L, Zang P, Guo Y, Wang X, Bailey ST, Jia Y. Automated diagnosis and segmentation of choroidal neovascularization in OCT angiography using deep learning. Biomed Opt Express 2020;11:927-44.
18. Bailey ST, Thaware O, Wang J, Hagag AM, Zhang X, Flaxel CJ, Lauer AK, Hwang TS, Lin P, Huang D, Jia Y. Detection of Nonexudative Choroidal Neovascularization and Progression to Exudative Choroidal Neovascularization Using OCT Angiography. Ophthalmol Retina 2019;3:629-36.
19. Faridi A, Jia Y, Gao SS, Huang D, Bhavsar KV, Wilson DJ, Sill A, Flaxel CJ, Hwang TS, Lauer AK, Bailey ST. Sensitivity and Specificity of OCT Angiography to Detect Choroidal Neovascularization. Ophthalmol Retina

2017;1:294-303.
20. Jia Y, Bailey ST, Wilson DJ, Tan O, Klein ML, Flaxel CJ, Potsaid B, Liu JJ, Lu CD, Kraus MF, Fujimoto JG, Huang D. Quantitative optical coherence tomography angiography of choroidal neovascularization in age-related macular degeneration. Ophthalmology 2014;121:1435-44.
21. Nesper PL, Soetikno BT, Zhang HF, Fawzi AA. OCT angiography and visible-light OCT in diabetic retinopathy. Vision Res 2017;139:191-203.
22. Guo Y, Hormel TT, Xiong H, Wang B, Camino A, Wang J, Huang D, Hwang TS, Jia Y. Development and validation of a deep learning algorithm for distinguishing the nonperfusion area from signal reduction artifacts on OCT angiography. Biomed Opt Express 2019;10:3257-68.
23. Hwang TS, Jia Y, Gao SS, Bailey ST, Lauer AK, Flaxel CJ, Wilson DJ, Huang D. Optical coherence tomography angiography features in diabetic retinopathy. Retina 2015;35:2371-6.
24. You QS, Guo Y, Wang J, Wei X, Camino A, Zang P, Flaxel CJ, Bailey ST, Huang D, Jia Y, Hwang TS. Detection of Clinically Unsuspected Retinal Neovascularization With Wide-Field Optical Coherence Tomography Angiography. Retina 2020;40:891-7.
25. Jia Y, Simonett JM, Wang J, Hua X, Liu L, Hwang TS, Huang D. Wide-field OCT angiography investigation of the relationship between radial peripapillary capillary plexus density and nerve fiber layer thickness. Invest Ophthalmol Vis Sci 2017;58:5188-94.
26. Liu L, Edmunds B, Takusagawa H, Tehrani S, Lombardi L, Morrison JC, Jia Y, Huang D. Projection-Resolved Optical Coherence Tomography Angiography of the Peripapillary Retina in Glaucoma. Am J Ophthalmol 2019;207:99-109.
27. Zhang S, Wu C, Liu L, Jia Y, Zhang Y, Zhang Y, Zhang H, Zhong Y, Huang D. Optical Coherence Tomography Angiography of the Peripapillary Retina in Primary Angle-Closure Glaucoma. Am J Ophthalmol 2017;182:194-200.
28. Jia Y, Wei E, Wang X, Zhang X, Morrison JC, Parikh M, Lombardi LH, Gattey DM, Armour RL, Edmunds B, Kraus MF, Fujimoto JG, Huang D. Optical coherence tomography angiography of optic disc perfusion in glaucoma. Ophthalmology 2014;121:1322-32.
29. Ghasemi Falavarjani K, Phasukkijwatana N, Freund KB, Cunningham ET, Kalevar A, McDonald HR, Dolz-Marco R, Roberts PK, Tsui I, Rosen R, Jampol LMEEM, Sadda SR, Ghasemi Falavarjani K, Phasukkijwatana N, Freund KB, Cunningham ET, Kalevar A, McDonald HR, Dolz-Marco R, Roberts PK, Tsui I, Rosen R, Jampol LMEEM, Sadda SR, Sarraf D. En Face Optical Coherence Tomography Analysis to Assess the Spectrum of Perivenular Ischemia and Paracentral Acute Middle Maculopathy in Retinal Vein Occlusion. Am J Ophthalmol 2017;177:131-8.
30. Tsuboi K, Sasajima H, Kamei M. Collateral Vessels in Branch Retinal Vein Occlusion: Anatomic and Functional Analyses by OCT Angiography. Ophthalmol Retina 2019;3:767-76.
31. Chidambara L, Gadde SGK, Yadav NK, Jayadev C, Bhanushali D, Appaji AM, Akkali M, Khurana A, Shetty R. Characteristics and quantification of vascular changes in macular telangiectasia type 2 on optical coherence tomography angiography. Br J Ophthalmol 2016;100:1482-8.
32. Hagag AM, Wang JIE, Lu K, Harman G, Weleber RG, Huang D, Yang P, Pennesi ME, Jia Y. Projection-Resolved Optical Coherence Tomographic Angiography of Retinal Plexuses in Retinitis Pigmentosa. Am J Ophthalmol 2019;204:70-9.
33. McClintic SM, Jia Y, Huang D, Bailey ST. Optical Coherence Tomographic Angiography of Choroidal Neovascularization Associated With Central Serous Chorioretinopathy. JAMA Ophthalmol 2015;133:1212-4.
34. Alabduljalil T, Patel RC, Alqahtani AA, Gao SS, Gale MJ, Zhang M, Jia Y, Huang D, Chiang PW, Chen R, Wang J, Weleber RG, Pennesi ME, Yang P. Correlation of Outer Retinal Degeneration and Choriocapillaris Loss in Stargardt Disease Using En Face Optical Coherence Tomography and Optical Coherence Tomography Angiography. Am J Ophthalmol 2019;202:79-90.
35. Battaglia Parodi M, Cicinelli MV, Rabiolo A, Pierro L, Gagliardi M, Bolognesi G, Bandello F. Vessel density analysis in patients with retinitis pigmentosa by means of optical coherence tomography angiography. Br J Ophthalmol 2017;101:428-32.
36. Durbin MK, An L, Shemonski ND, Soares M, Santos T, Lopes M, Neves C, Cunha-Vaz J. Quantification of retinal microvascular density in optical coherence tomographic angiography images in diabetic retinopathy. JAMA Ophthalmol 2017;135:370-6.
37. Hwang TS, Gao SS, Liu L, Lauer AK, Bailey ST, Flaxel CJ, Wilson DJ, Huang D, Jia Y. Automated quantification of capillary nonperfusion using optical coherence tomography angiography in diabetic retinopathy. JAMA Ophthalmol 2016;134:367-73.
38. Yarmohammadi A, Zangwill LM, Manalastas PIC, Fuller NJ, Diniz-Filho A, Saunders LJ, Suh MH, Hasenstab K, Weinreb RN. Peripapillary and Macular Vessel

Density in Patients with Primary Open-Angle Glaucoma and Unilateral Visual Field Loss. Ophthalmology 2018;125:578-87.
39. Holmen IC, Konda MS, Pak JW, Mcdaniel KW, Blodi B, Stepien KE, Domalpally A. Prevalence and Severity of Artifacts in Optical Coherence Tomographic Angiograms. JAMA Ophthalmol 2020;138:119-26.
40. Fercher AF, Hitzenberger CK, Kamp G, El-Zaiat SY. Measurement of intraocular distances by backscattering spectral interferometry. Optics Communications 1995;117:43-8.
41. Zhang A, Zhang Q, Chen CL, Wang RK. Methods and algorithms for optical coherence tomography-based angiography: a review and comparison. J Biomed Opt 2015;20:100901.
42. Vakoc B, Yun SH, de Boer JF, Tearney GJ, Bouma BE. Phase-resolved optical frequency domain imaging. Opt Express 2005;13:5483-93.
43. Wei X, Camino A, Pi S, Cepurna W, Huang D, Morrison JC, Jia Y. Fast and robust standard-deviation-based method for bulk motion compensation in phase-based functional OCT. Opt Lett 2018;43:2204-7.
44. Choi WJ, Qin W, Chen CL, Wang J, Zhang Q, Yang X, Gao BZ, Wang RK. Characterizing relationship between optical microangiography signals and capillary flow using microfluidic channels. Biomed Opt Express 2016;7:2709.
45. Su JP, Chandwani R, Gao SS, Pechauer AD, Zhang M, Wang J, Jia Y, Huang D, Liu G. Calibration of optical coherence tomography angiography with a microfluidic chip. J Biomed Opt 2016;21:86015.
46. Michelotti M, Zhang M, Hwang TS, Bailey ST, Flaxel CJ, Lauer A, Lin P, Campbell JP, Wilson DJ, Huang D, Jia Y. Motion Signal Detected in Cystic Spaces on Optical Coherence Tomography Angiography. Investigative Ophthalmology & Visual Science 2016;57:5453.
47. Kashani AH, Green KM, Kwon J, Chu Z, Zhang Q, Wang RK, Garrity S, Sarraf D, Rebhun CB, Waheed NK, Schaal KB, Munk MR, Gattoussi S, Freund KB, Zheng F, Liu G, Resenfeld PJ. Suspended Scattering Particles in Motion: A Novel Feature of OCT Angiography in Exudative Maculopathies. Ophthalmol Retina 2018;2:694-702.
48. Lu JQ, Yang P, Hu X-H. Simulations of light scattering from a biconcave red blood cell using the finite-difference time-domain method. J Biomed Opt 2005;10:024022.
49. Karlsson A, He J, Swartling J, Andersson-Engels S. Numerical simulations of light scattering by red blood cells. IEEE Transactions on Biomedical Engineering 2005;52:13-8.
50. Wang Q, Chan S, Yang JY, You B, Wang YX, Jonas JB, Wei WB. Vascular density in retina and choriocapillaris as measured by optical coherence tomography angiography. Am J Ophthalmol 2016;168:95-109.
51. Uji A, Balasubramanian S, Lei J, Baghdasaryan E, Al-Sheikh M, Sadda SR. Impact of Multiple En Face Image Averaging on Quantitative Assessment from Optical Coherence Tomography Angiography Images. Ophthalmology 2017;124:944-52.
52. Corvi F, Pellegrini M, Erba S, Cozzi M, Staurenghi G, Giani A. Reproducibility of Vessel Density, Fractal Dimension, and Foveal Avascular Zone Using 7 Different Optical Coherence Tomography Angiography Devices. Am J Ophthalmol 2018;186:25-31.
53. Zhang Q, Jonas JB, Wang Q, Chan SY, Xu L, Wei WB, Wang YX. Optical Coherence Tomography Angiography Vessel Density Changes after Acute Intraocular Pressure Elevation. Sci Rep 2018;8:6024.
54. Mitchell P, Liew G, Gopinath B, Wong TY. Age-related macular degeneration. Lancet 2018;392:1147-59.
55. Bhavsar KV, Jia Y, Wang J, Patel RC, Lauer AK, Huang D, Bailey ST. Projection-resolved optical coherence tomography angiography exhibiting early flow prior to clinically observed retinal angiomatous proliferation. Am J Ophthalmol Case Rep 2017;8:53-7.
56. Zhang A, Zhang Q, Wang RK. Minimizing projection artifacts for accurate presentation of choroidal neovascularization in OCT micro-angiography. Biomed Opt Express 2015;6:4130-43.
57. Zang P, Wang J, Hormel TT, Liu L, Huang D, Jia Y. Automated segmentation of peripapillary retinal boundaries in OCT combining a convolutional neural network and a multi-weights graph search. Biomed Opt Express 2019;10:4340.
58. Guo Y, Camino A, Zhang M, Wang J, Huang D, Hwang T, Jia Y. Automated segmentation of retinal layer boundaries and capillary plexuses in wide-field optical coherence tomographic angiography. Biomed Opt Express 2018;9:4429-42.
59. Wang J, Zhang M, Hwang TS, Bailey ST, Huang D, Wilson DJ, Jia Y. Reflectance-based projection-resolved optical coherence tomography angiography. Biomed Opt Express 2017;8:1536-48.
60. Zhang M, Hwang TS, Campbell JP, Bailey ST, Wilson DJ, Huang D, Jia Y. Projection-resolved optical coherence tomographic angiography. Biomed Opt Express 2016;7:816-28.
61. Patel RC, Wang J, Hwang TS, Zhang M, Gao SS, Pennesi

ME, Bailey ST, Lujan BJ, Wang X, Wilson DJ, Huang D, Jia Y. Plexus-Specific Detection of Retinal Vascular Pathologic Conditions with Projection-Resolved OCT Angiography. Ophthalmol Retina 2018;2:816-26.
62. Takusagawa HL, Liu L, Ma KN, Jia Y, Gao SS, Zhang M, Edmunds B, Parikh M, Tehrani S, Morrison JC, Huang D. Projection-Resolved Optical Coherence Tomography Angiography of Macular Retinal Circulation in Glaucoma. Ophthalmology 2017;124:1589-99.
63. Koyanagi Y, Murakami Y, Funatsu J, Akiyama M, Nakatake S, Fujiwara K, Tachibana T, Nakao S, Hisatomi T, Yoshida S, Ishibashi T, Sonoda KH, Ikeda Y. Optical coherence tomography angiography of the macular microvasculature changes in retinitis pigmentosa. Acta Ophthalmologica 2018;96:e59-67.
64. Takagi S, Hirami Y, Takahashi M, Fujihara M, Mandai M, Miyakoshi C, Tomita G, Kurimoto Y. Optical coherence tomography angiography in patients with retinitis pigmentosa who have normal visual acuity. Acta Ophthalmologica 2018;96:e636-42.
65. Coscas F, Glacet-Bernard A, Miere A, Caillaux V, Uzzan J, Lupidi M, Coscas G, Souied EH. Optical Coherence Tomography Angiography in Retinal Vein Occlusion: Evaluation of Superficial and Deep Capillary Plexa. Am J Ophthalmol 2016;161:160-71.e1.
66. Onishi AC, Nesper PL, Roberts PK, Moharram GA, Chai H, Liu L, Jampol LM, Fawzi AA. Importance of considering the middle capillary plexus on OCT angiography in diabetic retinopathy. Invest Ophthalmol Vis Sci 2018;59:2167-76.
67. Hwang TS, Hagag AM, Wang J, Zhang M, Smith A, Wilson DJ, Huang D, Jia Y. Automated Quantification of Nonperfusion Areas in 3 Vascular Plexuses With Optical Coherence Tomography Angiography in Eyes of Patients With Diabetes. JAMA Ophthalmol 2018;136:929-36.
68. McClintic SM, Gao S, Wang J, Hagag A, Lauer AK, Flaxel CJ, Bhavsar K, Hwang TS, Huang D, Jia Y, Bailey ST. Quantitative Evaluation of Choroidal Neovascularization under Pre Re Nata Anti-Vascular Endothelial Growth Factor Therapy with OCT Angiography. Ophthalmol Retina 2018;2:931-41.
69. de Oliveira Dias JR, Zhang Q, Garcia JMB, Zheng F, Motulsky EH, Roisman L, Miller A, Chen CL, Kubach S, de Sisternes L, Durbin MK, Feuer W, Wang RK, Gregori G, Rosenfeld PJ. Natural History of Subclinical Neovascularization in Nonexudative Age-Related Macular Degeneration Using Swept-Source OCT Angiography. Ophthalmology 2018;125:255-66.
70. Zhang Q, Wang RK, Chen CL, Legarreta AD, Durbin MK, An L, Sharma U, Stetson PF, Legarreta JE, Roisman L, Gregori G, Rosenfeld PJ. Swept source optical coherence tomography angiography of neovascular macular telangiectasia type 2. Retina 2015;35:2285-99.
71. Camino A, Zhang M, Dongye C, Pechauer AD, Hwang TS, Bailey ST, Lujan B, Wilson DJ, Huang D, Jia Y. Automated registration and enhanced processing of clinical optical coherence tomography angiography. Quant Imaging Med Surg 2016;6:391-401.
72. Camino A, Zhang M, Gao SS, Hwang TS, Sharma U, Wilson DJ, Huang D, Jia Y. Evaluation of artifact reduction in optical coherence tomography angiography with real-time tracking and motion correction technology. Biomed Opt Express 2016;7:3905-15.
73. Braaf B, Vienola KV, Sheehy CK, Yang Q, Vermeer KA, Tiruveedhula P, Arathorn DW, Roorda A, de Boer JF. Real-time eye motion correction in phase-resolved OCT angiography with tracking SLO. Biomed Opt Express 2013;4:51-65.
74. Ferguson RD, Hammer DX, Paunescu LA, Beaton S, Schuman JS. Tracking optical coherence tomography. Opt Lett 2004;29:2139-41.
75. Vienola KV, Braaf B, Sheehy CK, Yang Q, Tiruveedhula P, Arathorn DW, de Boer JF, Roorda A. Real-time eye motion compensation for OCT imaging with tracking SLO. Biomed Opt Express 2012;3:2950-63.
76. Zhang Q, Huang Y, Zhang T, Kubach S, An L, Laron M, Sharma U, Wang RK. Wide-field imaging of retinal vasculature using optical coherence tomography-based microangiography provided by motion tracking. J Biomed Opt 2015;20:066008.
77. Zang P, Liu G, Zhang M, Dongye C, Wang J, Pechauer AD, Hwang TS, Wilson DJ, Huang D, Li D, Jia Y. Automated motion correction using parallel-strip registration for wide-field en face OCT angiogram. Biomed Opt Express 2016;7:2823-36.
78. Zang P, Liu G, Zhang M, Wang J, Hwang TS, Wilson DJ, Huang D, Li D, Jia Y. Automated three-dimensional registration and volume rebuilding for wide-field angiographic and structural optical coherence tomography. J Biomed Opt 2017;22:26001.
79. Hendargo HC, Estrada R, Chiu SJ, Tomasi C, Farsiu S, Izatt JA. Automated non-rigid registration and mosaicing for robust imaging of distinct retinal capillary beds using speckle variance optical coherence tomography. Biomed Opt Express 2013;4:803-21.
80. Kraus MF, Liu JJ, Schottenhamml J, Chen C-L, Budai A,

Branchini L, Ko T, Ishikawa H, Wollstein G, Schuman J, Duker JS, Fujimoto JG, Hornegger J. Quantitative 3D-OCT motion correction with tilt and illumination correction, robust similarity measure and regularization. Biomed Opt Express 2014;5:2591-613.
81. Kraus MF, Potsaid B, Mayer MA, Bock R, Baumann B, Liu JJ, Hornegger J, Fujimoto JG. Motion correction in optical coherence tomography volumes on a per A-scan basis using orthogonal scan patterns. Biomed Opt Express 2012;3:1182-99.
82. Wei X, Hormel TT, Guo Y, Hwang TS, Jia Y. High-resolution wide-field OCT angiography with a self-navigation method to correct microsaccades and blinks. 2020;11:3234-45.
83. Makita S, Hong Y, Yamanari M, Yatagai T, Yasuno Y. Optical coherence angiography. Opt Express 2006;14:7821-40.
84. An L, Wang RK. In vivo volumetric imaging of vascular perfusion within human retina and choroids with optical micro-angiography. Opt Express 2008;16:11438-52.
85. An L, Shen TT, Wang RK. Using ultrahigh sensitive optical microangiography to achieve comprehensive depth resolved microvasculature mapping for human retina. J Biomed Opt 2011;16:106013.
86. Camino A, Zhang M, Liu L, Wang J, Jia Y, Huang D. Enhanced quantification of retinal perfusion by improved discrimination of blood flow from bulk motion signal in OCTA. Transl Vis Sci Technol 2018;7:20.
87. Camino A, Jia Y, Liu G, Wang J, Huang D. Regression-Based Algorithm for Bulk Motion Subtraction in Optical Coherence Tomography Angiography. Biomed Opt Express 2017;8:3053-66.
88. Gao SS, Jia Y, Liu L, Zhang M, Takusagawa HL, Morrison JC, Huang D. Compensation for reflectance variation in vessel density quantification by optical coherence tomography angiography. Invest Ophthalmol Vis Sci 2016;57:4485-92.
89. Yu JJ, Camino A, Liu L, Zhang X, Wang J, Gao SS, Jia Y, Huang D. Signal Strength Reduction Effects in OCT Angiography. Ophthalmol Retina 2019;3:835-42.
90. Niu S, Yu C, Chen Q, Yuan S, Lin J, Fan W, Liu Q. Multimodality analysis of hyper-reflective foci and hard exudates in patients with diabetic retinopathy. Sci Rep 2017;7:1568.
91. De Benedetto U, Sacconi R, Pierro L, Lattanzio R, Bandello F. Optical Coherence Tomographic Hyperreflective Foci in Early Stages of Diabetic Retinopathy. Retina 2015;35:449-53.
92. Cheng Y, Guo L, Pan C, Lu T, Hong T, Ding Z, Li P. Statistical analysis of motion contrast in optical coherence tomography angiography. J Biomed Opt 2015;20:116004.
93. Jian Y, Wong K, Sarunic MV. Graphics processing unit accelerated optical coherence tomography processing at megahertz axial scan rate and high resolution video rate volumetric rendering. J Biomed Opt 2013;18:26002.
94. Wei X, Camino A, Pi S, Hormel TT, Cepurna W, Huang D, Morrison JC, Jia Y. Real-time cross-sectional and en face OCT angiography guiding high-quality scan acquisition. Opt Lett 2019;44:1431.
95. Wei X, Hormel TT, Guo Y, Jia Y. 75-degree non-mydriatic single-volume optical coherence tomographic angiography. Biomed Opt Express 2019;10:6286-95.
96. Babcock HW. The Possibility of Compensating Astronomical Seeing. Publ Astron Soc Pac 1953;65:229.
97. Salas M, Augustin M, Ginner L, Kumar A, Baumann B, Leitgeb R, Drexler W, Prager S, Hafner J, Schmidt-Erfurth U, Pircher M. Visualization of micro-capillaries using optical coherence tomography angiography with and without adaptive optics. Biomed Opt Express 2016;8:207-22.
98. Wang Q, Kocaoglu OP, Cense B, Bruestle J, Jonnal RS, Gao W, Miller DT. Imaging retinal capillaries using ultrahigh-resolution optical coherence tomography and adaptive optics. Invest Ophthalmol Vis Sci 2011;52:6292-9.
99. Jiang Z, Huang Z, Qiu B, Meng X, You Y, Liu X, Liu G, Zhou C, Yang K, Maier A, Ren Q, Lu Y. Comparative study of deep learning models for optical coherence tomography angiography. Biomed Opt Express 2020;11:1580-97.
100. Liu X, Huang Z, Wang Z, Wen C, Jiang Z, Yu Z, Liu J, Liu G, Huang X, Maier A, Ren Q, Lu Y. A deep learning based pipeline for optical coherence tomography angiography. J Biophotonics 2019;12:e201900008.
101. Lee CS, Tyring AJ, Wu Y, Xiao S, Rokem AS, DeRuyter NP, Zhang Q, Tufail A, Wang RK, Lee AY. Generating retinal flow maps from structural optical coherence tomography with artificial intelligence. Sci Rep 2019;9:5694.

Cite this article as: Hormel TT, Huang D, Jia Y. Artifacts and artifact removal in optical coherence tomographic angiography. Quant Imaging Med Surg 2021;11(3):1120-1133. doi: 10.21037/qims-20-730

